ACCEPTED MANUSCRIPT

Electrical & Mechanical Diagnostic Indicators of Wind Turbine Induction Generator Rotor Faults

D. Zappalá[a,*], N. Sarma[b,1], S. Djurović[b], C. J. Crabtree[a], A. Mohammad[b], P. J. Tavner[a]

[a] Department of Engineering, Durham University, South Road, Durham, UK

[b] School of Electrical and Electronic Engineering, Power Conversion Group, The University of Manchester, Manchester, UK

[*] donatella.zappala@durham.ac.uk

Abstract:

In MW-sized wind turbines, the most widely-used generator is the wound rotor induction machine, with a partially-rated voltage source converter connected to the rotor. This generator is a significant cause of wind turbine fault modes. In this paper, a harmonic time-stepped generator model is applied to derive wound rotor induction generator electrical & mechanical signals for fault measurement, and propose simple closed-form analytical expressions to describe them. Predictions are then validated with tests on a 30 kW induction generator test rig. Results show that generator rotor unbalance produces substantial increases in the side-bands of supply frequency and slotting harmonic frequencies in the spectra of current, power, speed, mechanical torque and vibration measurements. It is believed that this is the first occasion in which such comprehensive approach has been presented for this type of machine, with healthy & faulty conditions at varying loads and rotor faults. Clear recommendations of the relative merits of various electrical & mechanical signals for detecting rotor faults are given, and reliable fault indicators are identified for incorporation into wind turbine condition monitoring systems. Finally, the paper proposes that fault detectability and reliability could be improved by data fusion of some of these electrical & mechanical signals.

Keywords: Wind Turbine; Condition Monitoring; Doubly-fed induction generator (DFIG); Electrical & mechanical signature analysis; Rotor Electrical unbalance; fault indicator

Declarations of interest: none

1. Introduction

Wind energy has a crucial role in providing sustainable energy. By the end of 2017, the world-wide wind power installed capacity has risen to 540 GW [1], of which 169 GW are in the EU, approximately 153 GW onshore and 16 GW offshore [2]. Offshore wind has significant generation potential in Europe, especially in the UK, thanks to beneficial wind resources and sea-bed conditions. Optimising operations and maintenance (O&M) strategy through the adoption of cost-effective and reliable condition monitoring (CM) techniques is a clear target for competitive offshore wind development [3][4][5]. One of the main challenges currently facing the wind CM

[1] Department of Electrical & Electronics Engineering, Duzce University, Duzce, Turkey

industry is to improve the reliability of diagnostic decisions, including component fault severity assessment [6]. Wound Rotor Induction Generators (WRIG), using a partially-rated Voltage Source Converter (VSC) to supply the rotor, known as Doubly-Fed Induction Generators (DFIG), are identified as the most widely-used generator in wind industry for MW-size variable speed applications [7][8], where Induction Generators in general are dominant, although Permanent Magnet Generators are gaining acceptance. Reliability surveys have highlighted that generator faults make a significant contribution to onshore wind turbine (WT) down-time [9][10][11]. With reduced accessibility offshore, any down-time is significantly extended. References [12][13][14] have also shown that rotor winding unbalance, caused by brush-gear or slip-ring wear/fault or winding electrical faults, are major contributors to WT generator failure rate. Monitoring generator electrical faults has not yet become standard practice in the wind industry where the majority of CM systems (CMS) are based on monitoring high-frequency vibration in gearbox and generator bearings [15]. Increasing concern about WT electrical component reliability [11], particularly offshore, could be overcome by expanding current CMS capabilities.

Steady-state DFIGs winding fault detection based on analysis of readily available current, power or even vibration signals has been widely researched and several diagnostic methods, based on time- or frequency-domain techniques, have been proposed to detect rotor failures. The first paper to consider current, speed and vibration measurement for detecting induction machine faults was [16] in 1982, in particular the presence of slip-dependant components in various induction machine electrical & mechanical signals has been reported in papers since 1978. However, more recent references [17]-[23] provide much greater analytical detail, at least for electrical signals. The feasibility of using mechanical signal spectra, vibration, torque or speed, as generator electrical unbalance fault indicators were investigated in [24]-[28]. However, all these papers relied on the analysis of single signals only, rather than considering the possibility of reducing effects of signal noise and improving detectability by combining multiple signals. The

adoption of a data fusion approach, based on the comparison of independent single signals, could contribute to increasing confidence and reduce false alarms, as already demonstrated for WT gearboxes in [29]-[31]. Despite interest in recognising generator fault signatures in multiple signals, there is a lack of literature explaining how to improve reliability by combining relevant diagnostic signals. Furthermore in WTs, the use of a VSC-connected machine monitored by a CMS now means that both electrical & mechanical signals are readily available to the operator.

This paper, therefore, sets out comprehensive generator signal prediction and measurement under rotor electrical unbalance (REU), at varying load and fault levels, with the aim of measuring wide-band, fault-related, electrical & mechanical harmonic side-bands, comparing and amalgamating them to improve fault recognition and raise reliability. The work builds on previous research [17][18][22][28][32], providing a comprehensive investigation of rotor electrical fault effects on DFIG stator current, I_s, power, P_e, shaft speed, N_s, mechanical torque, T_m & frame vibration, A_v.

First, the paper provides closed-form analytical expressions, arising from author's previous published work, linking fault-related signal frequencies to generator operating conditions. A harmonic model of a laboratory DFIG is then used to investigate REU wide-band spectral signatures. The extent to which fault-related frequencies, predicted by theory, are manifested in DFIG electrical & mechanical signals is then investigated experimentally. Finally, the correlation between the identified electrical & mechanical signal spectral components and their ability to demonstrate rotor fault severity progression within the generator operating range is explored with the aim of identifying reliable fault indicators for potential incorporation in commercial WT CMSs.

2. Generator Rotor Electrical Unbalance: Model Study

Closed-form analytical expressions defining the spectral characteristics of I_s & P_e, for a DFIG with an electrically balanced rotor were previously presented by the Authors in [17][28][32] and

are summarised in Table 1. These equations account for unbalanced stator supply and higher order field harmonics, typical of practical applications. According to [16][33][34], a spectral content of electro-magnetic origin is also detectable in the speed signal, N_s. Machine electrical & mechanical spectra under balanced conditions, described by equations in Table 1, are defined by a set of characteristic frequencies, referred to as carrier frequencies (CF). These frequencies are an artefact of generator design and supply harmonic content, and depend on: rotor slip (s), supply frequency (f), supply harmonic order (i and l, where i, l = 1,2,3…) and air-gap magnetic field pole pair number (k, where k = 1,2,3…). The CF expressions in Table 1 contain two distinct subgroups:

i. Supply frequency harmonic carriers (H), rotor speed invariant artefacts of supply harmonics, corresponding to $k = 0$ and $i \neq 0$ for current or $l \pm i \neq 0$ for other signals;
ii. Slot harmonic carriers (S), rotor speed dependant inter-harmonic frequencies due to slotting, corresponding to $k \neq 0$ and $i \neq 0$ for current or $l \pm i \neq 0$ for other signals.

Table 1 I_s, P_e & N_s, Carrier Frequencies (CF) and their ±2nsf side-bands

REU gives rise to additional $\pm 2nsf$ side-bands around existing CF components in I_s spectra, which are consequently reflected into counter-part $\pm 2nsf$ components of the CFs identified in the P_e & N_s spectra [22][28][33][34][35], where n can take any positive integer value, i.e. n = 0, 1, 2, 3… The third column in Table 1 summarises analytical expressions describing possible DFIG signal spectral content under REU operation, derived by taking account of CFs $2nsf$ side-bands, i.e. CF$\pm 2nsf$. As side-bands generally decay with order [22], only fundamental (i.e. first order side-band) components are examined further in this work. REU-induced side-band equations can be resolved into two distinct sub-groups depending on whether they correspond to supply harmonic side-bands (H_L and H_U) or slot harmonic side-bands (S_L and S_U), where subscripts L and U denote lower and upper $2sf$ CF side-bands, respectively.

To understand REU-induced electrical & mechanical spectra, a time-stepped DFIG harmonic model was developed [18][36]. A 4-pole laboratory generator has been used in this research; the model emulated its design and operational data as model inputs. The model enables the analysis of higher order harmonic effects and was used to study the steady-state spectral content of I_s, P_e & N_s signals. Generator operation was simulated for illustration purposes at the loaded operating speed of 1590 rpm, 90 rpm above synchronous speed and speed-ripple effects were incorporated in model calculations [33][34]. The three-phase supply was modelled with 3% magnitude unbalance to match typical laboratory levels. The stator windings were modelled as balanced for the purposes of this study. To study the spectral effects of interest predicted spectra were investigated over 0-450 Hz band-width for I_s & P_e, and 0-150 Hz band-width for N_s. The harmonic model was used to evaluate the influence of supply harmonics on signal spectra for the generator operating with an electrically balanced rotor using wide-band modelling of dominant 3^{rd}, 5^{th}, 7^{th}, 11^{th} and 13^{th} supply harmonics, $H_{1+3+5+7+11+13}$, with mean rms value limits, in terms of fundamental percentage, of 5%, 6%, 5%, 3.5% and 3%, respectively, as specified in the relevant grid code [40].

Predictions were obtained from the model to evaluate wide-band REU spectral signatures by increasing one rotor phase winding resistance by 300% of its rated value.

The predicted stator phase current, I_s, total power, P_e and generator speed, N_s, under balanced and unbalanced, 300% REU, conditions are shown in Figs 1 & 2. For each signal direct comparison of healthy and faulty spectra enables a clear understanding of REU wide-band spectra.

Supply harmonic carriers derived from I_s and P_e & N_s have been denoted by HI and HP, respectively; while slotting harmonic carriers have been denoted by SI and SP, respectively. For clarity, only REU first order side-band frequencies are labelled in Figs 1 & 2, where the subscripts L and U denote CF *2sf* lower and upper side-bands, respectively, identified by the red solid lines for H harmonic side-bands and by the blue dotted lines for S slot harmonic side-bands.

Fig. 1. Predicted I_s (a) & P_e (b) spectra at 1590 rpm

Spectral frequencies labelled in the graphs can be calculated for corresponding operating conditions by appropriate expressions in Table 1. This confirms the validity of the proposed closed-form equations for analysis of REU induced spectral signature. Tables 2-5 list equation parameters and corresponding spectral frequency numeric values observed in model results.

Fig. 2. Predicted N_s speed spectra, 1590 rpm, Balanced rotor winding & 300% REU

Table 2 Predicted I_s supply frequency harmonics and their side-bands

Table 3 Predicted I_s slotting harmonics and their side-bands

Table 4 Predicted P_e & N_s supply frequency harmonics and their side-bands

Table 5 Predicted P_e & N_s slotting harmonics and their side-bands

3. Generator Rotor Electrical Unbalance: Experimental validation

3.1. Experimental Test Rig

Model results were experimentally validated and quantified in a series of experiments on a laboratory test rig, illustrated in Fig. 3, comprising an industrial 4-pole, three phase, 240 V, 50 Hz, 30 kW, star-connected WRIG. The generator rotor rated phase resistance was 0.066Ω. The WRIG was mechanically coupled with a 40 kW DC generator, used to drive the WRIG at a pre-chosen constant speed during experiments. The generator stator windings were connected to the grid via a three phase variable transformer, whilst the rotor windings were short-circuited. REU conditions were emulated by introducing additional resistance into one rotor phase winding.

Fig. 3. Schematic diagram of the experimental test rig and its instrumentation

The DC generator speed and torque were controlled by a commercial DC controller. A shaft mounted 1024 ppr incremental encoder was used for speed measurement and its output signals processed in real-time using a dSPACE 1103 platform to extract the value of N_s. WRIG instantaneous stator currents, I_s, and voltages, V, were measured using Hall effect sensors and synchronously recorded by a LeCroy WaveSurfer digital oscilloscope sampling at a rate of 10 kHz. Recorded currents and voltages were used to calculate the total

instantaneous stator power, P_e, using the two wattmeter method. The WRIG was mounted on a Kistler 9281B force platform, containing three-axis piezoelectric transducers, to measure the dynamic shaft torque [37]. The piezoelectric sensor signals were acquired by a NI DAQ-6351 card and then processed to calculate the shaft torque, T_m. The WRIG frame vibration, A_v, was measured on the horizontal axis with a Brüel&Kjaer (B&K) DT4394 piezoelectric accelerometer, which was fitted to the generator load-side end-plate. The vibration spectrum was recorded with 0-1 kHz band-width at 6400 lines of resolution using a B&K PULSE vibration analysis platform. Other signals were processed using the MATLAB FFT routine with 2^{17} data points to achieve a frequency resolution of 0.0763 Hz/line. Monitored signals were recorded during generator steady-state operation and their spectra examined for this study over a 0-450 Hz band-width for I_s, P_e, T_m & A_v signals, and over a 0-150 Hz band-width for N_s.

3.2. Electrical & Mechanical Signal Analysis

To allow direct comparison with model predictions presented in Section 2, tests were first performed at 1590 rpm. An external additional resistance of ≈0.198Ω was introduced into one rotor phase to give up to 300% REU. I_s, P_e & N_s spectra measured for healthy and faulty conditions are shown in Figs 4 & 5. Detectable frequencies of interest, corresponding to $\pm 2sf$ side-bands tabulated in Tables 2-5, are labelled in the measurements. Measured spectra are in good agreement with predictions, where contents originating from supply-induced inter-harmonic effects, slotting side-bands and REU side-bands are shown. As predicted by analysis reported in section 2, the presented measurements confirm that REU causes additional, slip-dependant side-bands at calculable frequencies, confirming this research.

a Measured I_s, Balanced rotor winding & 300% REU
b Measured P_e, Balanced rotor winding & 300% REU

Fig. 4. Measured I_s & P_e at 1590 rpm

Small discrepancies between numerical and experimental results are due to inherent supply frequency variations and velocity measurement accuracy limitations. Some REU-related side-bands are present in the healthy generator spectra, at low magnitude, as an artefact of inherent rotor unbalance, unavoidable in any practical generator, arising from manufacturing imperfections [17]. Measurements are also much noisier than model predictions due to inevitable geometrical inaccuracies in machine construction and the full air-gap electro-magnetic effects, as well as supply secondary noise effects not represented in the model for the sake of clarity. However, most predicted REU-specific components are clearly visible above measurement noise. Comparison between healthy and faulty spectra indicates that REU induces considerable change in many components, with I_s & P_e side-bands giving clearer fault indication than N_s.

Fig. 5. Measured N_s at 1590 rpm, Balanced rotor winding & 300% REU

4. Discussion

4.1. Model Study

Model predictions in Fig 2 and Tables 2-5 show the presence of significant wide-band signatures in all I_s, P_e & N_s generator signals. For operation under REU conditions additional $\pm 2nsf$ side-band components clearly arise in supply and slot harmonic spectral components that can be correlated across different signals. Previous work [25][26][28][32][38] has shown that effects associated with attractive rotor-stator radial magnetic forces can also give rise to oscillations at identical frequencies in T_m & A_v as in P_e & N_s spectra. In summary, models identified the following components to be looked for in experimental signals:

- SI, HI lower and upper *2sf* side-bands in I_s;
- SP & HP lower and upper *2sf* side-bands in P_e, N_s, T_m & A_v, respectively.

These side-bands correspond to those disparately described in previous literature, presented comprehensively in this model study.

4.2. Experimental Study

I_s, P_e & N_s model predictions are confirmed by the experimental results presented in Section 3.2 and shown in Fig 4 for I_s & P_e and Fig 5 for N_s. Fig 6 shows the experimental results for T_m & A_v. Note that, in this case, the same side-band labelling system as for P_e & N_s has been adopted to indicate the detectable $\pm 2sf$ frequencies.

a T_m, Balanced rotor windings & 300% REU

b A_v, Balanced rotor windings &300% REU

Fig. 6. Measured T_m & Av at 1590 rpm

Inherent rotor unbalance artefacts, due to manufacturing imperfections in practical generators [17], give rise to low magnitude $\pm 2sf$ side-bands in T_m & A_v even under healthy operation; this is expected and clearly seen in Fig**.** 6. T_m & A_v spectra are noisier than corresponding electrical signals, partly due to the mechanical instrumentation but also because A_v is affected by both air-gap excitation and frame response [26][38][39]. The majority of REU-related supply frequency harmonic and slotting component $\pm 2sf$ side-bands, predicted by the model, are clearly visible in measured T_m spectra but because of the dependency of the vibrations on the generator frame mechanical response, not all frequencies observed in T_m are manifested in A_v. A_v shows similar but non-identical characteristics, compared to I_s, P_e, T_m & N_s because, whilst the air-gap flux density is modulated by the fault harmonics, vibration signals are also attenuated by the resonant vibration response of the machine stator core and frame, as described in [16][28]. Slotting harmonic (SP) side-bands together with HP_{1U}, in the case of T_m, and with HP_{3U}, in the case of A_v, are most prominent and, in most cases, exhibit clear increases under generator fault conditions. The upper $2sf$ side-band of the fundamental harmonic at zero Hz, HP_{1U}, traditionally used as an REU indicator [41], is invisible in A_v spectra because of the limited frequency response of the piezoelectric accelerometer, i.e. 5 Hz-10 kHz; a similar constraint will exist in commercial CMS sensors [15].

Table 6 summarises the detectable supply and slotting harmonic side-bands in I_s, P_e, N_s, T_m & A_v measured signals, present in REU faults, derived directly from the generator air-gap flux density, modulated by rotor fault harmonics, and in A_v affected by frame response.

Table 6 Measured P_e, I_s, T_m, N_s & A_v supply, H, and slotting, S, harmonic side-bands showing presence of REU faults, taken from Figs 4-6, based on faults predicted in Tables 2-5

4.3. Fault Detection

The influence of REU severity and generator load on the fault recognition capability of identified ±*2sf* side-bands has been investigated by performing a series of tests under steady-state conditions over the full generator operating range. The WRIG speed was increased in steps of 30 rpm, from no-load, 1500 rpm, up to full-load, 1590 rpm. At each steady-state load, the generator was first tested under balanced rotor conditions and then under three increasing severity REU levels, shown in

Table 7. The REU level was estimated as a percentage of balanced phase resistance, comparable to those used in previous studies [19][21][24].

Table 7 REU progressively introduced into one rotor phase circuit

For each fault and load condition, five separate I_s, V, N_s & A_v measurements and four separate *Tm* measurements were recorded. The fault signal spectra examined in steady-state agreed with the predicted and experimental results described in Sections 2 & 3. The magnitudes of ±*2sf* fault-related side-bands, identified in Table 6, were extracted from each signal and averaged to minimise sensitivity to supply variations. A normalised detectability algorithm, *D*, applied to the measured data has been defined as:

$$D = \frac{\sum_i F_i^2}{\sum_i H_i^2} \quad (1)$$

where:

- $\sum_i F_i^2$ is the sum of amplitudes squared of selected fault condition CF harmonic side-bands;

- $\sum_i H_i^2$ is the sum of amplitudes squared of selected unfaulted condition CF harmonic side-bands.

Results were then compared, in Fig 7, to investigate the ability of each identified component to discriminate fault severity over the full generator operating range, based on the harmonics listed in Table 6. Note that *D* has a floor level of 1 when $\sum_i F_i^2 = \sum_i H_i^2$, as indicated in Fig 7 graphs by the grey base to ordinate *D*.

a, I_s *b*, P_e

c, N_s *d*, T_m

e, A_v

Fig. 7. Normalised Detectability, *D*, from various separate electrical & mechanical signals, from Table 6, for varying load and rotor fault severity

In Fig 7 I_s & P_e show the most distinct responses to REU changes, even for small fault magnitudes; T_m also exhibits clear rising trends, with an exception at 1530 rpm, while N_s also provides a reliable fault indicator, although with lower sensitivity as unbalance increases. Fig 7.e shows that vibration, A_v, did not exhibit side-bands giving consistent fault recognition within the generator operating range, due to the A_v-REU signature being attenuated by generator frame mechanical response, which, in this case, varies significantly with operating speed [28]. In addition the accelerometer frequency response in these experiments could not identify HP_{1U} vibration components. Fault recognition using this side-band could be possible if low frequency resolution accelerometers, such as fibre optics, were employed.

4.4. Improving Fault Detectability by Data Fusion

Various authors have advocated data fusion to improve fault detectability, notably for wind turbine gearboxes [30] and electrical machines [41]. The principal of data fusion is to increase detectability and detection confidence for the condition monitor and maintainer by combining signals from different sources. The suitability of combining REU-specific frequencies in generator signals as CMS fault indicators for data fusion can be assessed

using the experimental load-dependency discussed in Section 4.3. The signals considered for data fusion from this paper, are with justification:

- Electrical, I_s or P_e, attractive as these signals are strong, closely related to the air-gap magnetic field and hence to REU*;*
- Mechanical, T_m, N_s or A_v, attractive as these signals come from reliable sources, trusted by generator operators, but less closely related to the air-gap magnetic field and hence REU.

The combination of I_s & A_v, P_e & N_s and I_s & T_m has been investigated. In each case, the combined normalised detectability, D_f, has been calculated by applying simplistic additive data fusion as:

$$D_f = \left(\frac{\sum_i F_i^2}{\sum_i H_i^2}\right)_e + \left(\frac{\sum_i F_i^2}{\sum_i H_i^2}\right)_m \quad (2)$$

where $\left(\frac{\sum_i F_i^2}{\sum_i H_i^2}\right)_e$ and $\left(\frac{\sum_i F_i^2}{\sum_i H_i^2}\right)_m$ are the normalised detectability of the electrical and mechanical signal, respectively, calculated using equation (1). The results of this simplistic additive data fusion are shown in Fig 8, to the same scale as Fig 7.

a, I_s & A_v

b, P_e & N_s

c, I_s & T_m

Fig. 8. Normalised Detectability, D_f, from data fusion of selected electrical & mechanical signals, for varying load and rotor fault severity

Fig 8 demonstrates that each considered simple additive data fusion of electrical & mechanical signals delivers increased detectability with consistent behaviour over a range of REU fault sizes and WRIG loads, plus increased robustness and confidence for the operator. More complex data fusion algorithms could be developed, dependant on experience and the response features of a given system being monitored.

5. Conclusions

This paper presents an investigation of electrical & mechanical signatures for DFIG rotor electrical unbalance (REU), identifying the best diagnostic reliability condition monitoring indicators. It is shown that by simple additive data fusion of specific electrical & mechanical signatures fault detectability can be enhanced with the following specific conclusions:

- Closed-form analytic expressions defining electrical & mechanical signal spectral content for healthy and faulty operating conditions have been derived and validated, by comparison between model predictions and tests on a fully instrumented 30 kW WRIG laboratory test rig. A comprehensive study of DFIG REU electrical & mechanical spectral signatures has been made using this high fidelity laboratory test system.
- It has been shown that the magnitude of slip-dependant side-bands of a wide range of both supply frequency and slotting harmonics show significant experimental increases under faulty REU conditions.
- Specific side-bands, of current, power, torque and speed, giving clear fault recognition, have been identified and give consistent behaviour across the generator operating range. They will be high diagnostic reliability indicators of REU.
- Experimental results show that REU produces consistent, high fault and load sensitivity current $\pm 2sf$ side-band spectral increases around slotting harmonic components, in addition to traditionally used upper $2sf$ side-band of the fundamental supply harmonic component.
- In the case of P_e, T_m & N_s signals DC component $2sf$ side-bands have been shown to be the most sensitive and reliable REU fault indicators. However, in the case of P_e, T_m, other side-bands of supply frequency and slotting related spectral components are also responsive to REU.
- Vibration signals, A_v, also exhibit the presence of REU as $2sf$ side-bands, clearly detectable in the vibration spectra. However those side-bands show less consistent fault level recognition

across the generator operating range, because of the effect of frame response. This suggests that, in addition to conventional electrical signals, mechanical A_v, T_m & N_s signals could be monitored to diagnose generator electrical fault severity or progression over time.

- Simplistic additive data fusion of simultaneous electrical & mechanical signals real-time side-bands has demonstrated enhanced REU fault recognition sensitivity and could be used in a CMS to allow assessment of damage severity. This has been confirmed experimentally in this paper for electrical & mechanical signal combinations of I_s & A_v, P_e & N_s or I_s & T_m. Confirmatory fault data from disparate sources increases robustness and confidence and would be a crucial step for successfully implementing condition-based maintenance.

Further work would be required to investigate how to apply the information in this paper to a practical wind turbine generator CMS system and propose more developed methods of data fusion than presented here to improve damage severity assessment.

6. Acknowledgments

This work was funded as part of the UK EPSRC SUPERGEN Wind Hub, EP/L014106/1.

7. References

[1] GWEC, 'Global wind statistics – 2017' (Global Wind Energy Council, 2018), pp.1-4.
[2] EWEA, 'Wind in power 2017 European Statistics' (European Wind Energy Association, 2018), pp. 1-26.
[3] Garcia Marquez, F.P., Tobias, A.M., Pinar Perez, J.M. *et al.*: 'Condition monitoring of wind turbines: techniques and methods', Renewable Energy, 2012, **46**, pp. 169-178.
[4] BVG Associates, 'Pathways to cost reduction in offshore wind technology: technology workstream' (The Crown Estate, 2012), pp. 1-232.
[5] Coronado, D., Fischer, K., 'Condition monitoring of wind turbines: state of the art, user experience and recommendations' (Fraunhofer Institute for Wind Energy and Energy System Technology IWES, 2015), pp. 1-83.
[6] Crabtree, C.J., Zappalá, D., Hogg, S.I.: 'Wind energy: UK experiences and offshore operational challenges', Proceedings of the Institution of Mechanical Engineers, Part A: Journal of Power and Energy, 2015, **229**, (7), pp. 727-746.
[7] Tavner, P.J.: 'Offshore Wind Turbines: Reliability, Availability & Maintenance' (Institution of Engineering and Technology, 2012, 1st ed.).
[8] Arántegui, R.L., '2013 JRC wind status report - Technology, market and economic aspects of wind energy in Europe,' EC, 2014.
[9] Ribrant, J., Bertling, L.M.: 'Survey of failures in wind power systems with focus on Swedish wind power plants during 1997-2005', IEEE Transactions on Energy Conversion, 2007, **22**, (1), pp.167-73.

[10] Tavner, P.J., Faulstich, S., Hahn, B. *et al.*: 'Reliability & availability of wind turbine electrical & electronic components', EPE Journal, 2010, **20**, (4), pp. 45-50.
[11] Wilkinson, M., Hendriks, B., Spinato, F. *et al.*: 'Methodology and Results of the ReliaWind Reliability Field Study'. Proc. Scientific Track of the European Wind Energy Association Conference, Warsaw, Poland, 2010.
[12] Alewine, K., Chen, W.: 'Wind turbine generator failure modes analysis and occurrence'. Proc. Windpower, Dallas, Texas, May 2010, pp. 1-6.
[13] Alewine, K., Chen, W.: 'A review of electrical winding failures in wind turbine generators'. Proc. IEEE Electrical Insulation Conference (EIC), Annapolis, MD, USA, June 2011, pp. 392-397.
[14] Carroll, J., McDonald, A., McMillian, D.: 'Reliability comparison of wind turbines with DFIG and PMG drive trains', IEEE Transactions on Energy Conversion, 2015, **30**, (2), pp. 663-670.
[15] Crabtree, C.J., Zappalá, D., Tavner, P.J.: 'Survey of commercially available condition monitoring systems for wind turbines' (Durham University and the SUPERGEN Wind Energy Technologies Consortium, 2014), pp. 1-22.
[16] Hargis, C, Gaydon, B.G., Kamash, K.: The detection of rotor defects in induction motors. IEE Conf. Publ. 213, 1982, pp. 216-220.
[17] Williamson, S., Djurović, S.: 'Origins of stator current spectra in DFIGs with winding faults and excitation asymmetries'. Proc. IEEE International Electric Machines and Drives Conference, IEMDC '09, Miami, USA, 2009, pp 563-570.
[18] Djurović, S., Williamson, S. Renfrew, A.: 'Dynamic model for doubly-fed induction machines with unbalanced excitation, both with and without winding faults', IET Electric Power Applications, 2009, **3**, (3), pp.171-177.
[19] Yazidi, A., Capolino, G.A., Filippetti, F. *et al.*: 'A new monitoring system for wind turbines with doubly-fed induction generators'. Proc. MELECON 2006 - 2006 IEEE Mediterranean Electrotechnical Conference, Malaga, 2006, pp. 1142-1145.
[20] Riera-Guasp, M., Antonino-Daviu, J.A., Capolino, G.A.: 'Advances in electrical machine, power electronic, and drive condition monitoring and fault detection: state of the art'. IEEE Transactions on Industrial Electronics, 2015, **62**, (3), pp. 1746-1759.
[21] Gritli, Y., Rossi, C., Casadei, D. *et al.*: 'Square current space–vector signature analysis for rotor fault detection in wound-rotor induction generator'. Proc. IEEE XXII International Conference on Electrical Machines, ICEM 2016. Lausanne, Switzerland, September 2016, pp. 2896-2900.
[22] Djurović, S., Crabtree, C. J., Tavner, P. J. *et al.*: 'Condition monitoring of wind turbine induction generators with rotor electrical asymmetry', IET Renewable Power Generation, 2012, **6**, (4), pp. 207-216.
[23] Artigao, E., Honrubia-Escribano A., Gomez-Lazaro E.: 'Current signature analysis to monitor DFIG wind turbine generators: A case study'. Renewable Energy, 2018, **116**, (B), pp. 5-14.
[24] Hsu J.S.: 'Monitoring of defects in induction motors through air-gap torque observation', IEEE Trans. Ind. Appl., 1995, **31**, (5), pp. 1016–1021.
[25] Ding, F., Trutt, F.C.: 'Calculation of frequency spectra of electromagnetic vibration for wound-rotor induction generators with winding faults', Electric Generators & Power Systems, 1988, **14**, (3-4), pp. 137–150
[26] Trutt, F.C., Sottile, J., Kohler, J.L.: 'Detection of AC machine winding deterioration using electrically excited vibrations', IEEE Transactions on Industry Applications, 2001, **37**, (1), pp. 10–14
[27] Rodriguez P.J., Belahcen A., Arkkio A.: 'Signatures of electrical faults in the force distribution and vibration pattern of induction motors', Proc. Inst. Electr. Eng. – Electr. Power Appl., 2006, **153**, p. 523.

[28] Djurović, S., Vilchis-Rodriguez, D.S., Smith, A.C.: 'Investigation of wound rotor induction generator vibration signal under stator electrical fault conditions', The IET Journal of Engineering, 2014, **4**, pp. 719-729.

[29] Feng, Y., Qiu, Y., Crabtree, C.J. *et al.*: 'Monitoring wind turbine gearboxes', Wind Energy, 2013, **16**, (5), pp. 728-740.

[30] Dempsey, P.J., Sheng, S.: 'Investigation of data fusion applied to health monitoring of wind turbine drive train components', Wind Energy, 2013, **16**, (4), pp. 479-489.

[31] Soua S., Van Lieshout P., Perera A. *et al.*: 'Determination of the combined vibrational and acoustic emission signature of a wind turbine gearbox and generator shaft in service as a pre-requisite for effective condition monitoring', Renewable Energy, 2013, **51**, pp. 175-181.

[32] Djurović, S., Vilchis-Rodriguez, D.S., Smith, A.C.: 'Supply induced inter-harmonic effects in wound rotor and doubly-fed induction generators', IEEE Transactions on Energy Conversion, 2015, **30**, (4), pp. 1397 - 1408.

[33] Filippetti, F., Franceschini, G., Tassoni, C., *et al.*: 'AI techniques in induction machines diagnosis including the speed ripple effect', IEEE Transactions on Industry Applications, 1998, **34**, (1), pp. 98-108.

[34] Djurović, S., Williamson, S.: 'Investigation of the impact of speed-ripple and inertia on the steady-state current spectrum of a DFIG with unbalanced rotor'. Proc. 5th IET International Conference on Power Electronics, Machines and Drives (PEMD), Brighton, UK, April 2010.

[35] Kral, C., Pirker, F., Pascoli, G.: 'The impact of inertia on rotor fault effects - theoretical aspects of the Vienna monitoring method', IEEE Transactions on Power Electronics, 2008, **23**, (4), pp. 2136-2142.

[36] Sarma, N., Tshiloz, K., Vilchis-Rodriguez, D.S. *et al.*: 'Modelling of induction generator time and space harmonic effects in the SIMULINK environment'. Proc. 2015 IEEE International Electric Machines and Drives Conference (IEMDC), Coeur d'Alene, ID, USA, May 2015, pp. 1279-1285.

[37] Healey, R.C., Lesley S., Williamson S. *et al.*: 'The measurement of transient electromagnetic torque in high performance electrical drives'. Proc. Sixth Int. Conf. Power Electronics and Variable Speed Drives, Nottingham, UK, 1996, pp. 226–229.

[38] Finley, W.R., Hodowanec, M.M., W. G. Holter: 'An analytical approach to solving motor vibration problems'. Proc. Industry Applications Society 46th Annual Petroleum and Chemical Technical Conference (Cat.No. 99CH37000), San Diego, CA, 1999, pp. 217-232.

[39] Djurović, S., Vilchis-Rodriguez, D.S., Smith, A.C.: 'Vibration monitoring for wound rotor induction generator winding fault detection'. Proc. XXth International Conference on Electrical Machines (ICEM), Marseille, France, September 2012, pp. 1-6.

[40] EN 50160: 'Voltage characteristics of electricity supplied by public distribution systems', 2010.

[41] Tavner, P.J., Ran, L., Penman, J., Sedding, H.: 'Condition Monitoring of Rotating Electrical Machines', Institution of Engineering and Technology, 2008, 2nd ed.

ACCEPTED MANUSCRIPT

ACCEPTED MANUSCRIPT

Table 1 I_s, P_e & N_s, Carrier Frequencies (CF) and their ±2nsf side-bands

Generator Signal	**Closed-Form Analytical Expressions**	
	Balanced Rotor (CF)	**Unbalanced Rotor (CF ± *2nsf*)**
Stator Current, I_s	$\lvert i \pm 6k(1-s)\rvert f$	$\lvert (i \pm 2ns) \pm 6k(1-s)\rvert f$
Stator Active Power, Rotational Speed, P_e & N_s	$\lvert [l \pm i] \pm 6k(1-s)\rvert f$	$\lvert ([l \pm i] \pm 2ns) \pm 6k(1-s)\rvert f$

ACCEPTED MANUSCRIPT

ACCEPTED MANUSCRIPT

Table 2 Predicted I_s supply frequency harmonics and their side-bands

i	*k*	**Supply Harmonic Carrier Frequencies (CF) HI**		**Supply Harmonic CF Side-bands**			
		CF	**Hz**	**CF+*2sf***	**Hz**	**CF-*2sf***	**Hz**
1	0	HI_1	50	HI_{1L}	44	HI_{1U}	56
3	0	HI_3	150	HI_{3L}	144	HI_{3U}	156
5	0	HI_5	250	HI_{5L}	244	HI_{5U}	256
7	0	HI_7	350	HI_{7L}	344	HI_{7U}	356

ACCEPTED MANUSCRIPT

Table 3 Predicted I_s slotting harmonics and their side-bands

i	*k*	**Slotting Harmonic Carrier Frequencies (CF) SI**		**Slotting Harmonic CF Side-bands**			
		CF	**Hz**	**CF+*2sf***	**Hz**	**CF-*2sf***	**Hz**
1	1	SI_1	268	SI_{1L}	262	SI_{1U}	274
1	1	SI_2	368	SI_{2L}	362	SI_{2U}	374

ACCEPTED MANUSCRIPT

Table 4 Predicted P_e & N_s supply frequency harmonics and their side-bands

i	*l*	*k*	**Supply Harmonic Carrier Frequencies (CF) HP**		**Supply Harmonic CF Side-bands**			
			CF	**Hz**	**CF+*2sf***	**Hz**	**CF-*2sf***	**Hz**
1	1	0	HP_1	0			HP_{1U}	6
3	1	0	HP_3	100	HP_{3L}	94	HP_{3U}	106
5	1	0	HP_5	200	HP_{5L}	194	HP_{5U}	206
7	1	0	HP_{7a}	300	HP_{7aL}	294	HP_{7aU}	306
7	1	0	HP_{7b}	400	HP_{7bL}	394	HP_{7bU}	406

ACCEPTED MANUSCRIPT

Table 5 Predicted P_e & N_s slotting harmonics and their side-bands

i	*l*	*k*	**Slotting Harmonic Carrier Frequencies (CF) SP**		**Slotting Harmonic CF Side-bands**			
			CF	**Hz**	**CF+*2sf***	**Hz**	**CF-*2sf***	**Hz**
1	1	1	SP_1	218	SP_{1L}	212	SP_{1U}	224
1	1	1	SP_2	318	SP_{2L}	312	SP_{2U}	324
1	1	1	SP_3	418	SP_{3L}	412	SP_{3U}	424

ACCEPTED MANUSCRIPT

Table 6 Measured P_e, I_s, T_m, N_s & A_v supply, H, and slotting, S, harmonic side-bands showing presence of REU faults, taken from Figs 4-6, based on faults predicted in Tables 2-5

		$\boldsymbol{I_s}$	$\boldsymbol{P_e}$	-
Electrical Signals	Supply frequency harmonic side-bands	HI_{1U} HI_{3U} HI_{5U} HI_{7U}	HP_{1U} HP_{3L} , HP_{3U} HP_{5U} HP_{7aL}, HP_{7aU}	-
	Slotting side-bands	SI_{1L}, SI_{1U} SI_{2L}, SI_{2U}	SP_{1L} SP_{2L}, SP_{2U}	-
		$\boldsymbol{N_s}$	$\boldsymbol{T_m}$	$\boldsymbol{A_v}$
Mechanical Signals		HP_{1U}	HP_{1U} HP_{7aU}	 HP_{3U} HP_{7bL}
	Slotting side-bands		SP_{1U} SP_{2L}, SP_{2U} SP_{3L}	 SP_{2L}, SP_{2U} SP_{3L}

ACCEPTED MANUSCRIPT

ACCEPTED MANUSCRIPT

Table 7 REU progressively introduced into one rotor phase circuit

Additional Phase Resistance [Ω]	REU Level [%]
0.099	150
0.1485	225
0.198	300

ACCEPTED MANUSCRIPT

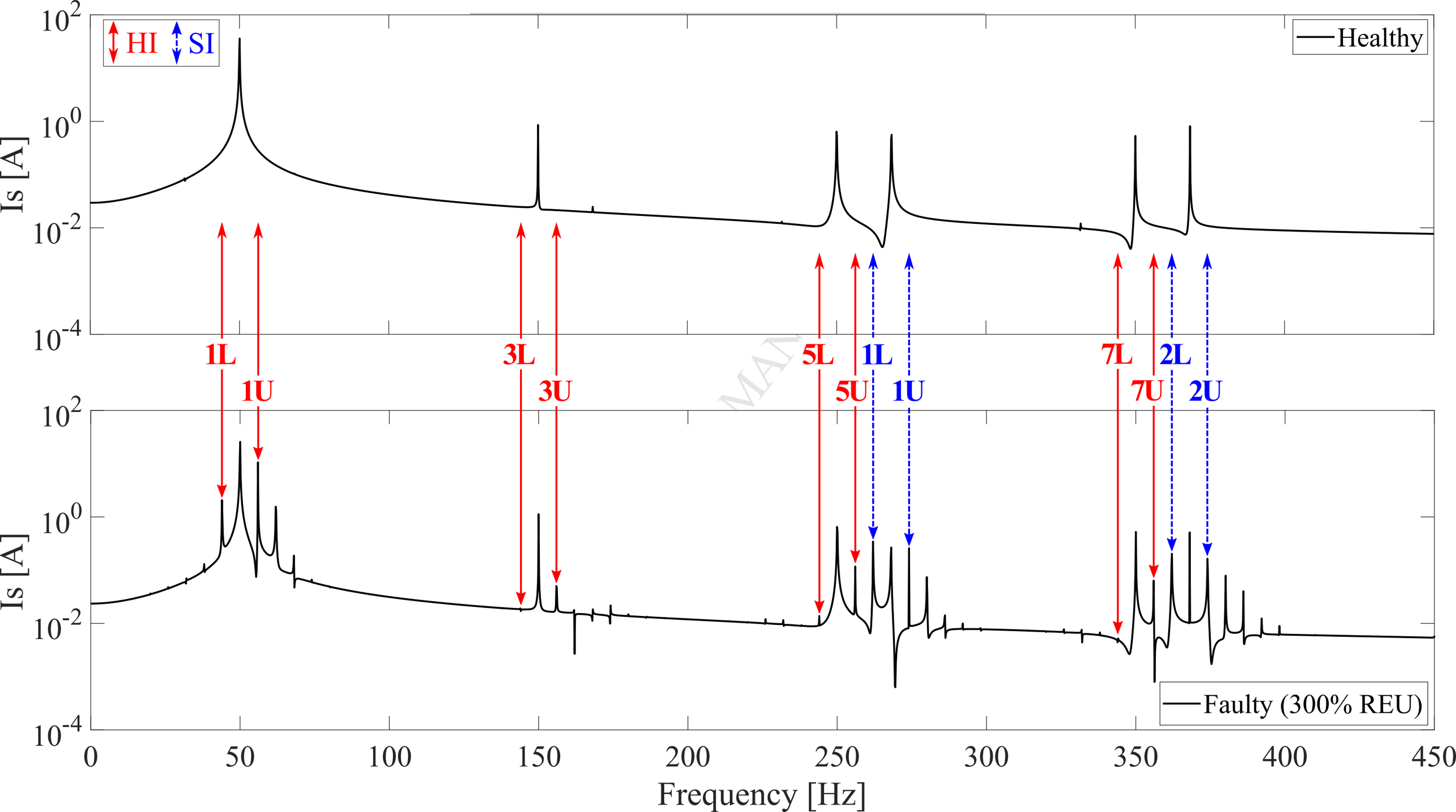
HI
SI
Healthy
Faulty (300% REU)
Is [A]
Frequency [Hz]
1L
1U
3L
3U
5L
5U
1L
1U
7L
7U
2L
2U

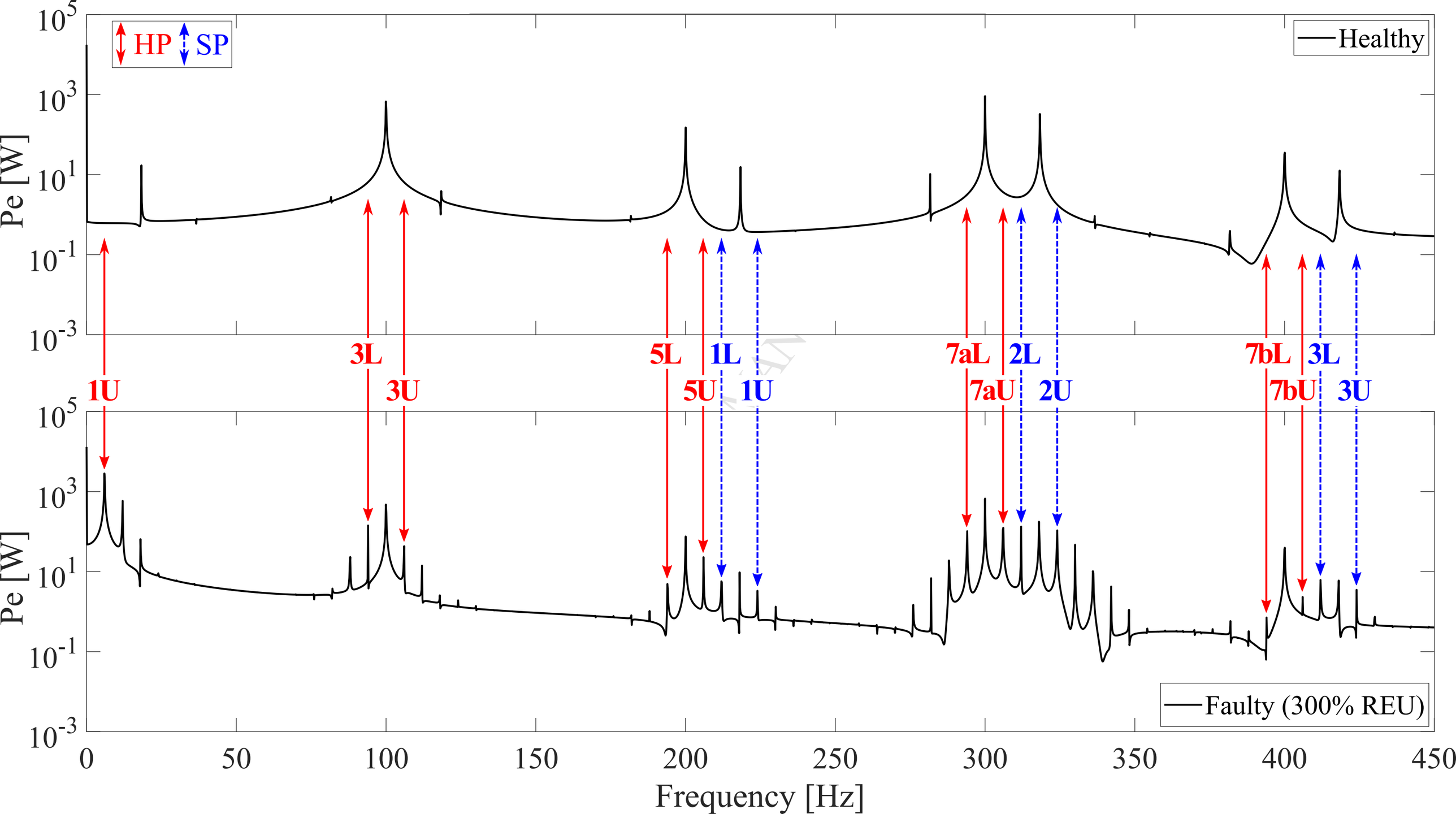
HP
SP
Healthy
Faulty (300% REU)
Pe [W]
Pe [W]
Frequency [Hz]
1U
3L
3U
5L
5U
1L
1U
7aL
7aU
2L
2U
7bL
7bU
3L
3U

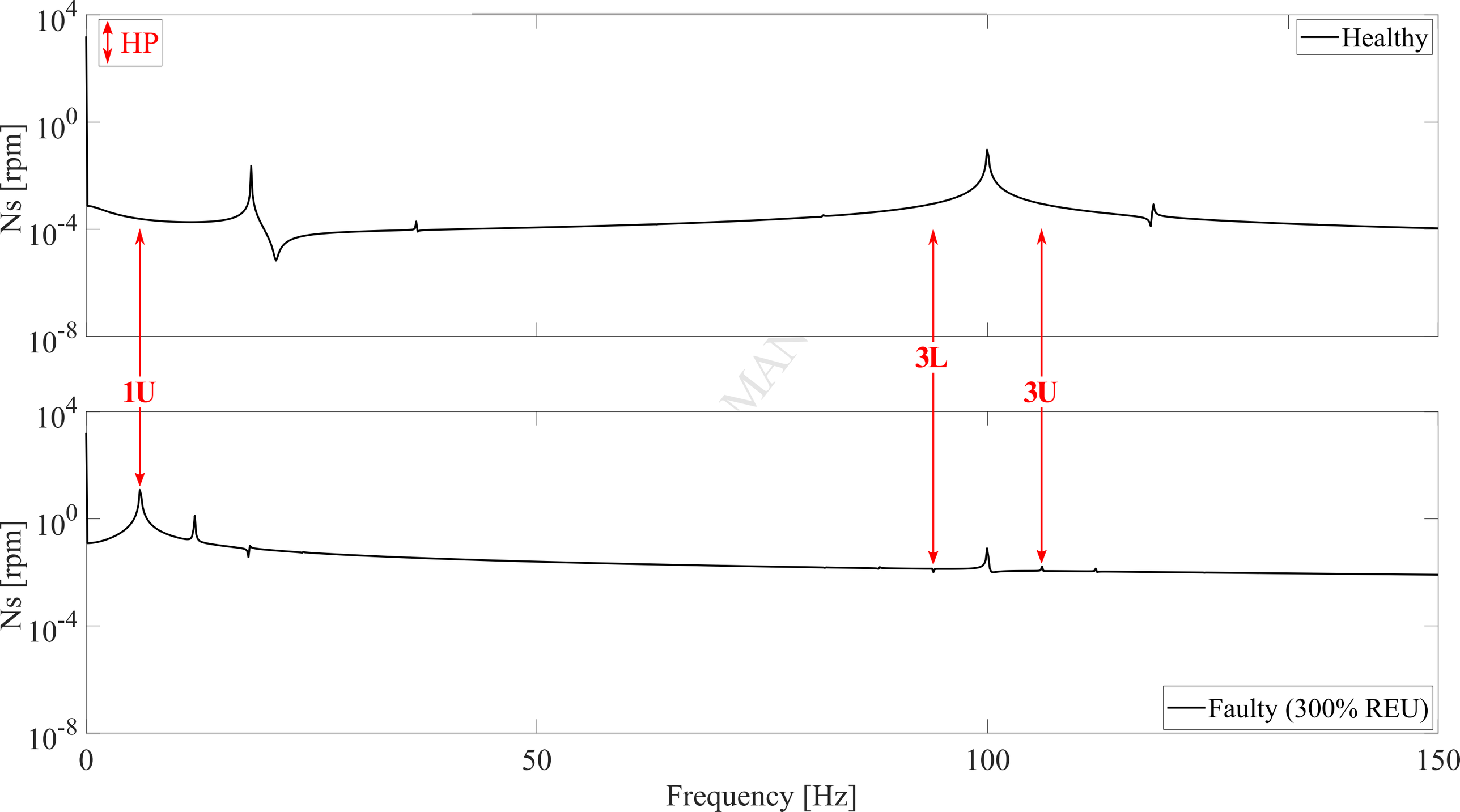
HP
Healthy
1U
3L
3U
Faulty (300% REU)
Ns [rpm]
Ns [rpm]
10^{4}
10^{0}
10^{-4}
10^{-8}
10^{4}
10^{0}
10^{-4}
10^{-8}
0
50
100
150
Frequency [Hz]

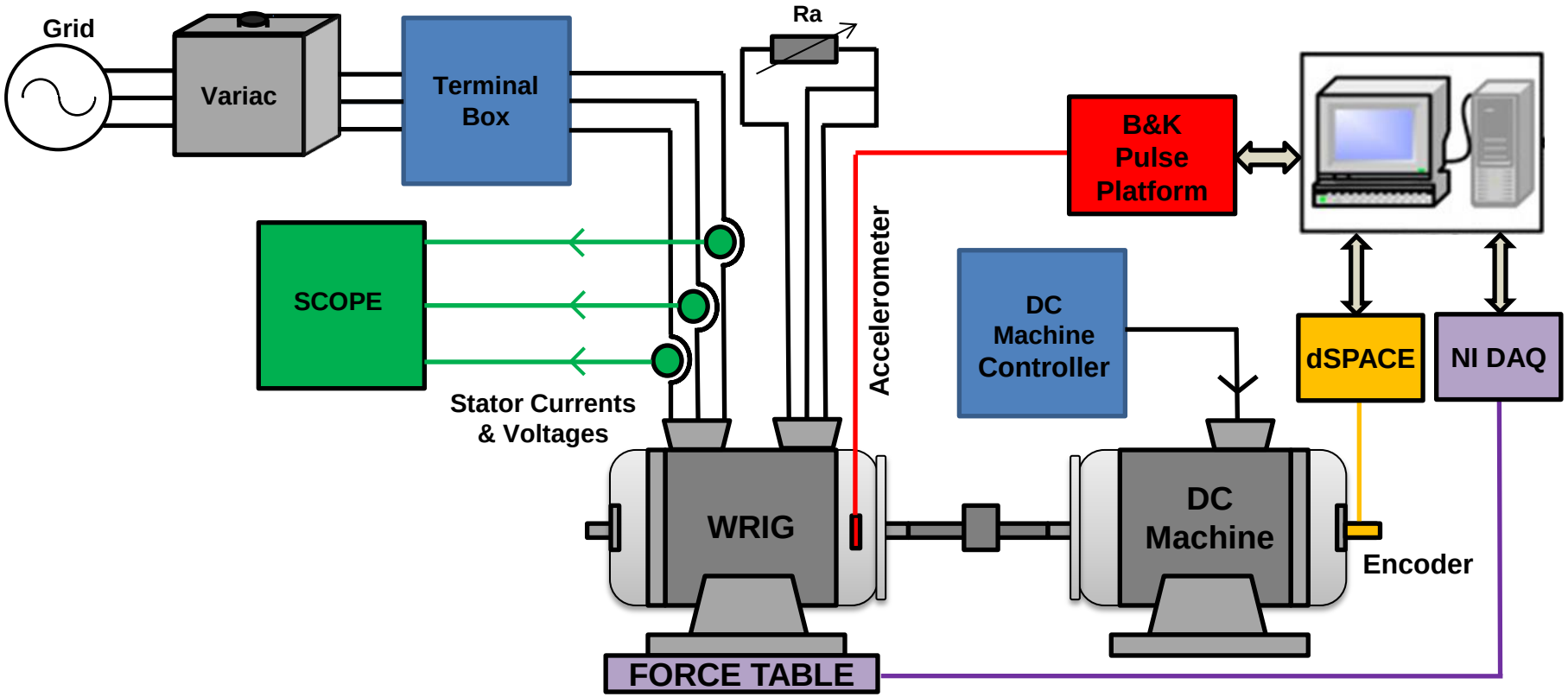
Grid
Variac
Terminal Box
Ra
B&K Pulse Platform
SCOPE
Accelerometer
DC Machine Controller
dSPACE
NI DAQ
Stator Currents & Voltages
WRIG
DC Machine
Encoder
FORCE TABLE

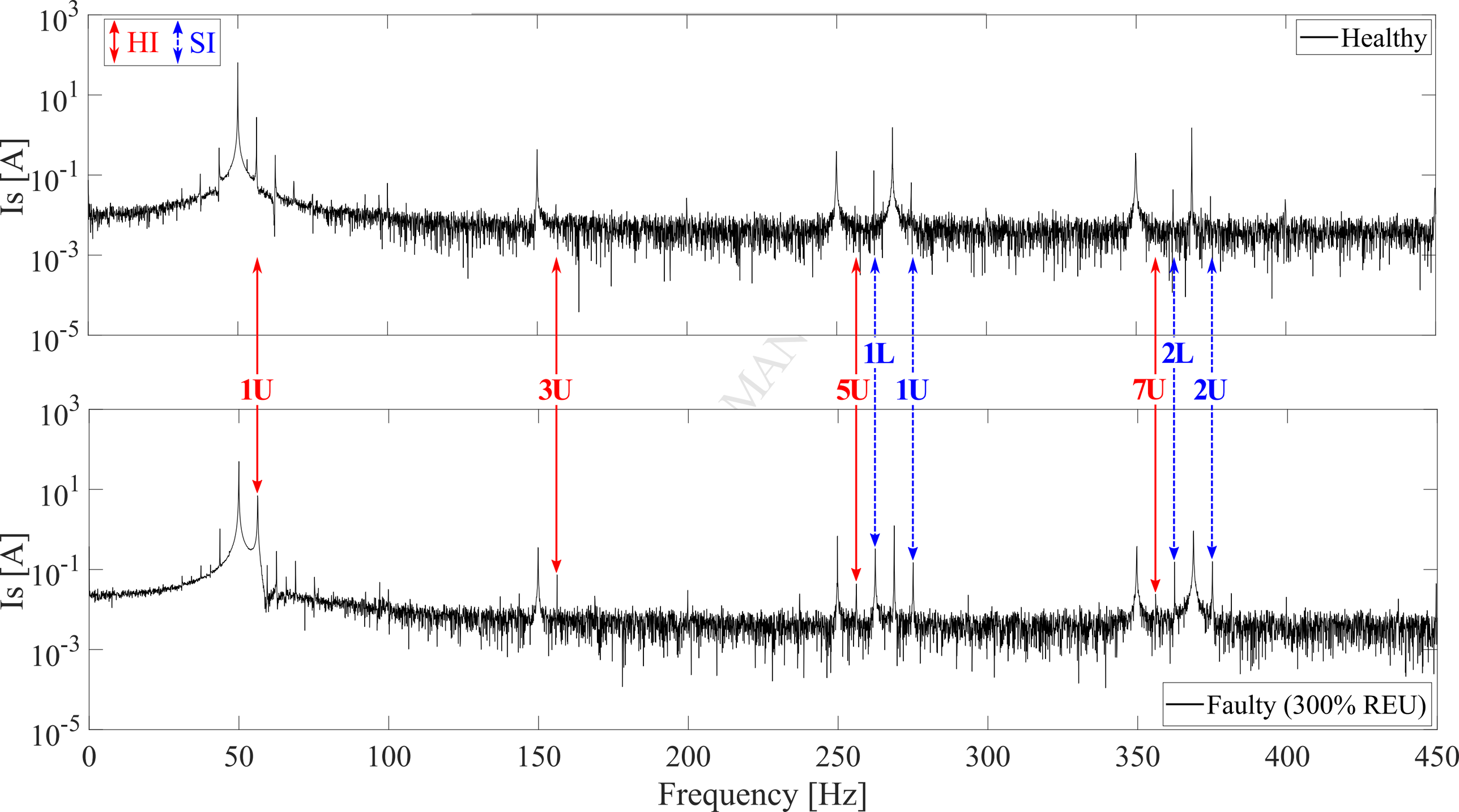
HI
SI
Healthy
Faulty (300% REU)
Is [A]
Frequency [Hz]
1U
3U
5U
1L
1U
7U
2L
2U
10^{3}
10^{1}
10^{-1}
10^{-3}
10^{-5}
0
50
100
150
200
250
300
350
400
450

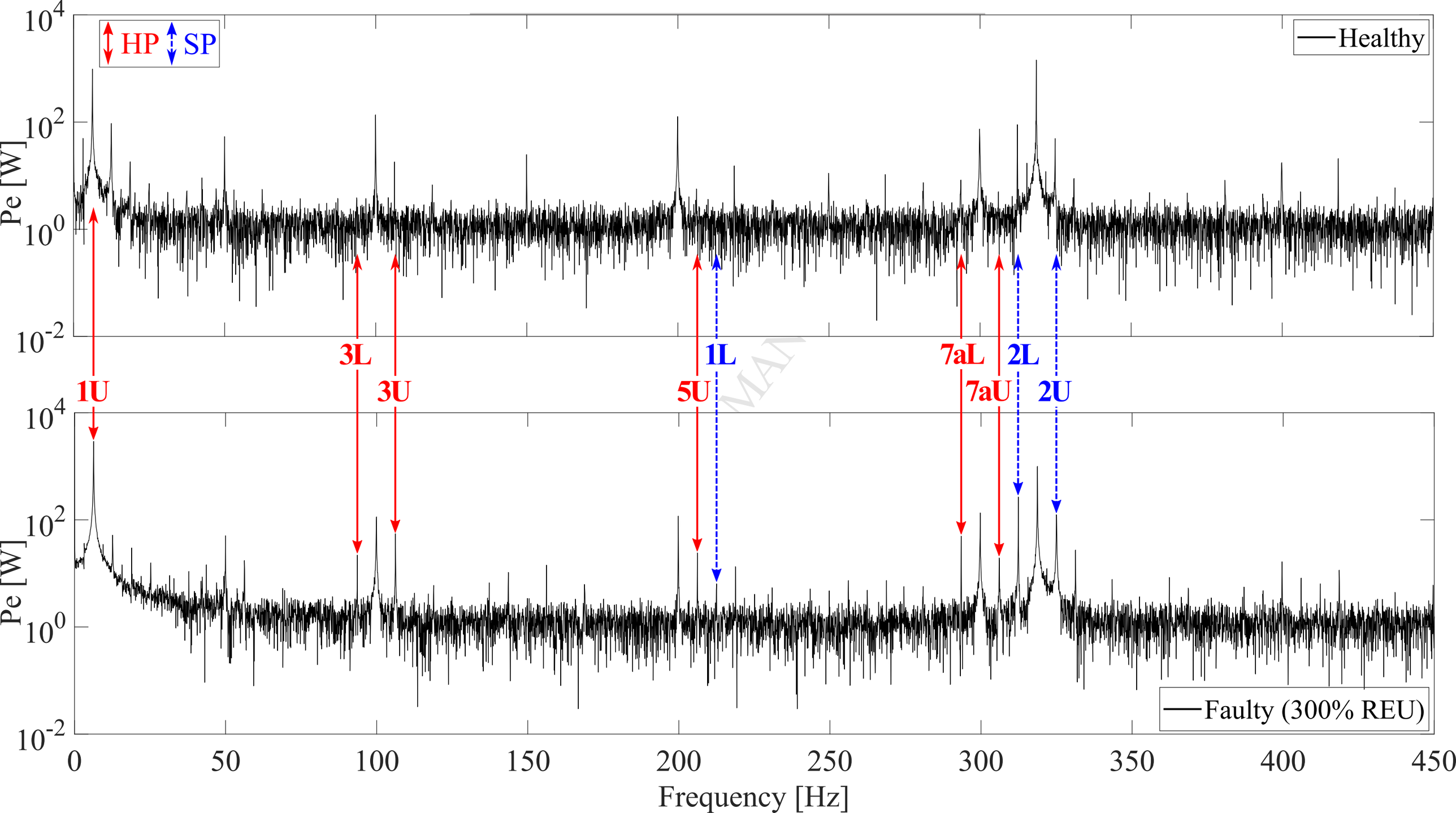
HP
SP
Healthy
Faulty (300% REU)
Pe [W]
Frequency [Hz]
1U
3L
3U
5U
1L
7aL
7aU
2L
2U
10^{4}
10^{2}
10^{0}
10^{-2}
0
50
100
150
200
250
300
350
400
450

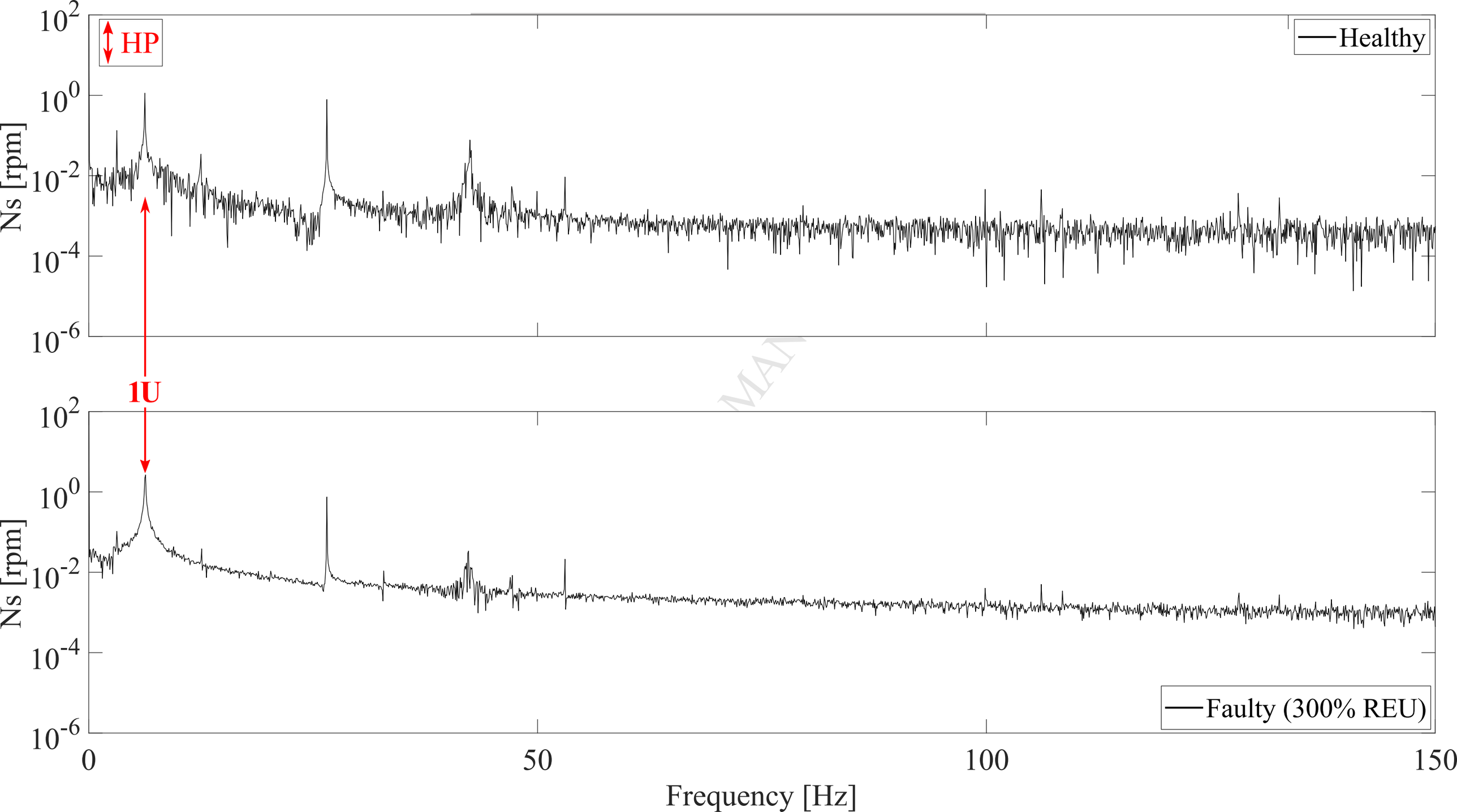
HP
Healthy
1U
Faulty (300% REU)
Ns [rpm]
Ns [rpm]
10^{2}
10^{0}
10^{-2}
10^{-4}
10^{-6}
10^{2}
10^{0}
10^{-2}
10^{-4}
10^{-6}
0
50
100
150
Frequency [Hz]

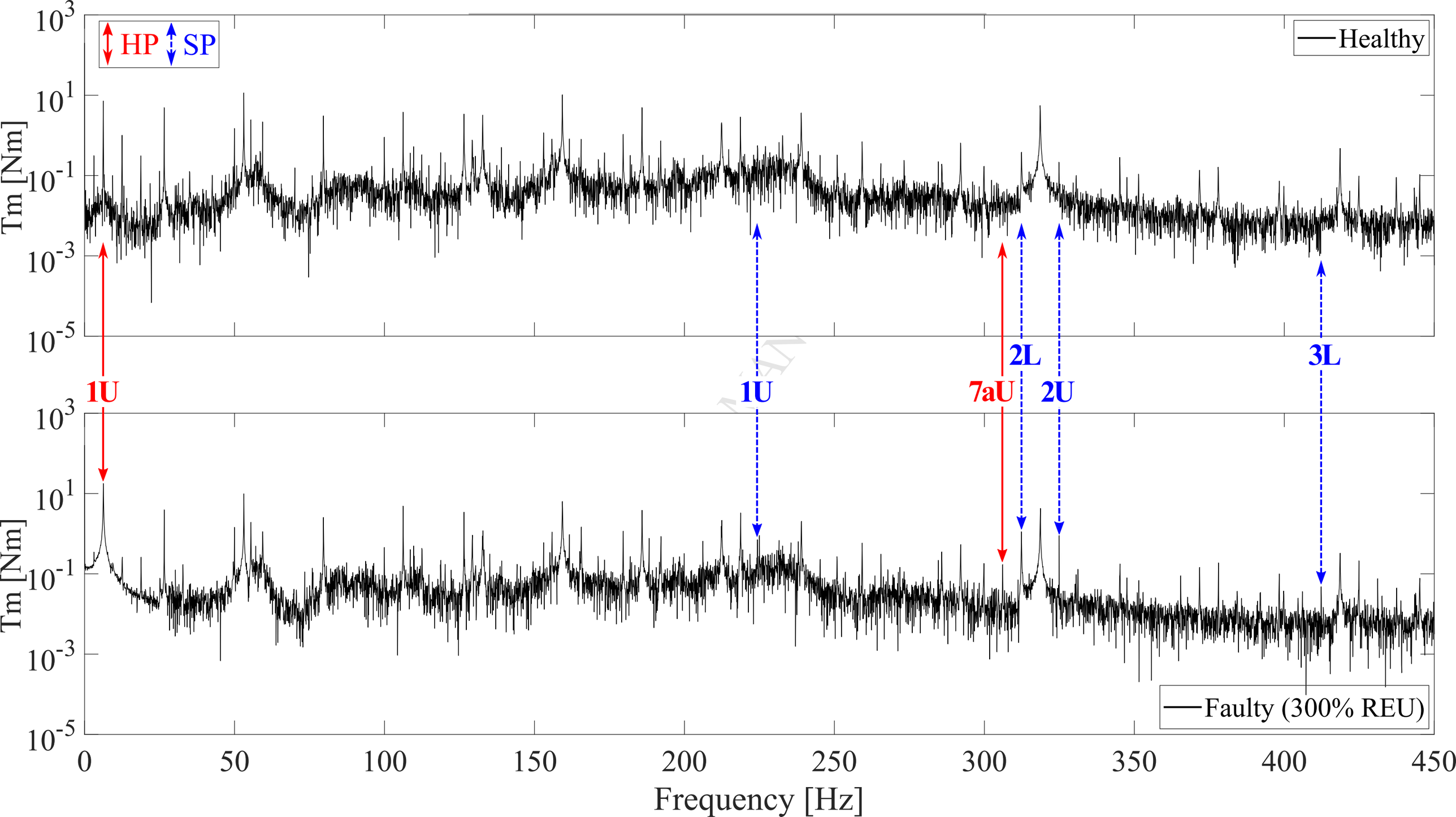
HP
SP
Healthy
Tm [Nm]
1U
1U
7aU
2L
2U
3L
Faulty (300% REU)
Frequency [Hz]

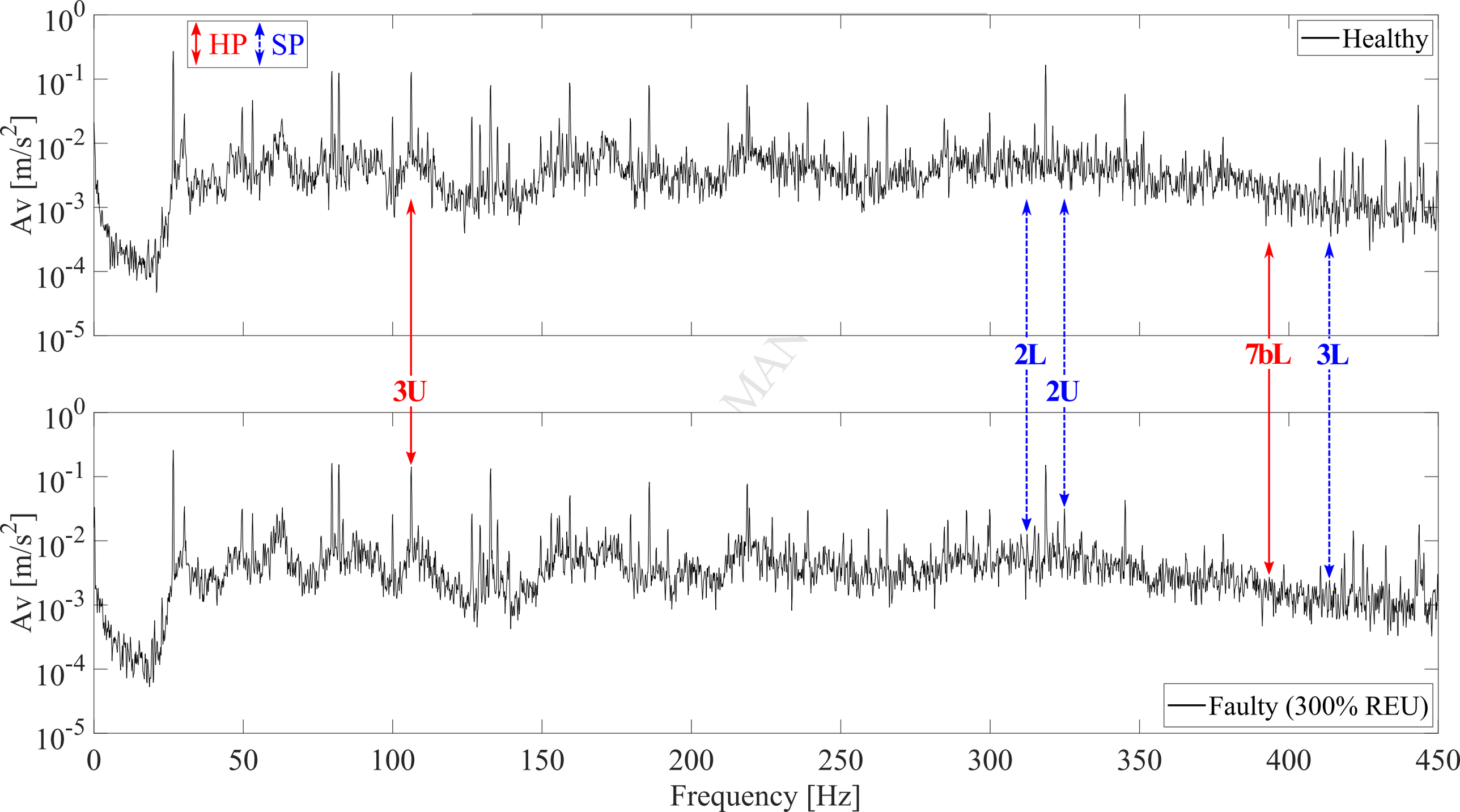
HP
SP
Healthy
Av [m/s^2]
10^{0}
10^{-1}
10^{-2}
10^{-3}
10^{-4}
10^{-5}
3U
2L
2U
7bL
3L
Faulty (300% REU)
0
50
100
150
200
250
300
350
400
450
Frequency [Hz]

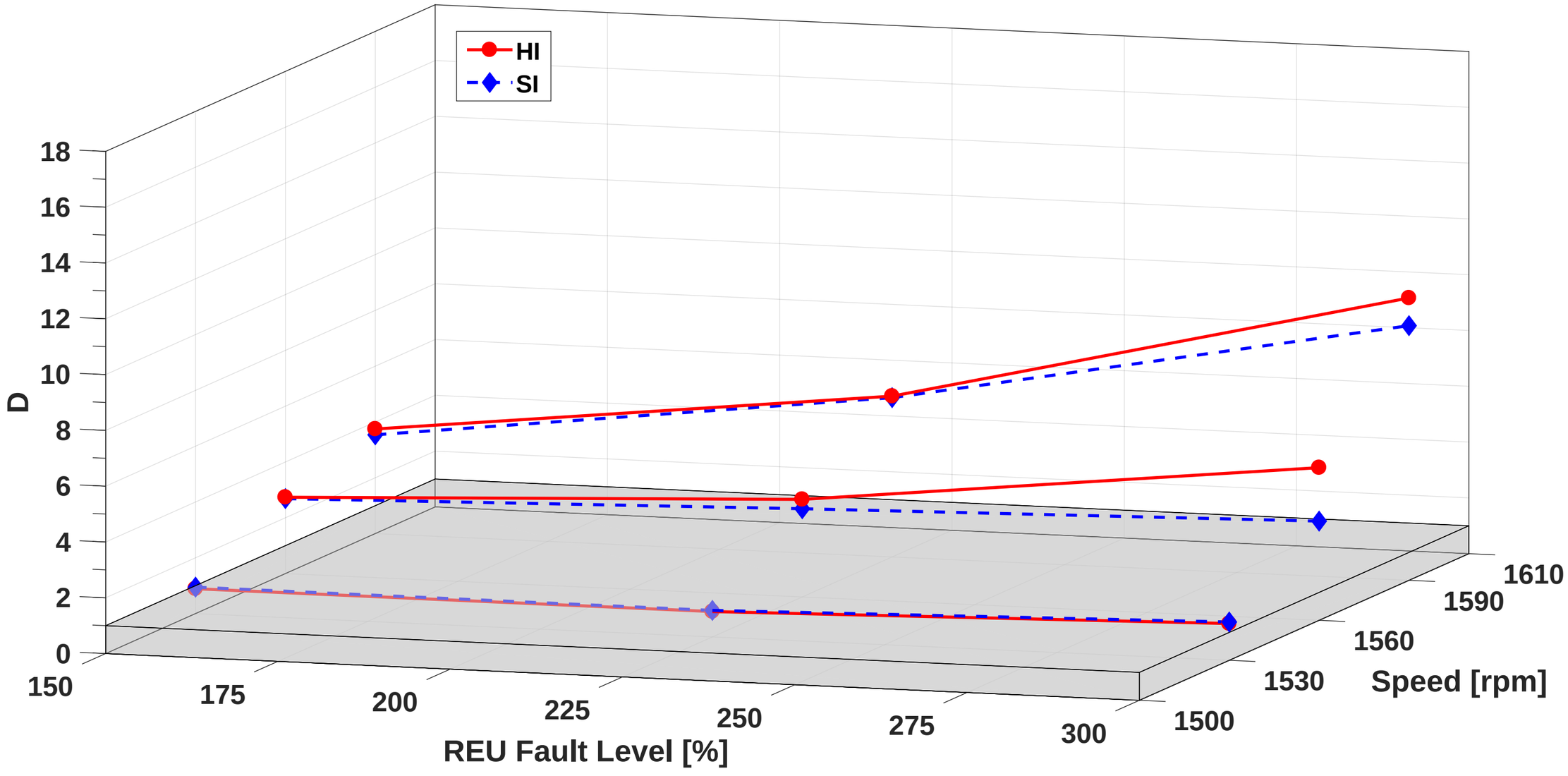
HI
SI
D
0
2
4
6
8
10
12
14
16
18
150
175
200
225
250
275
300
REU Fault Level [%]
1500
1530
1560
1590
1610
Speed [rpm]

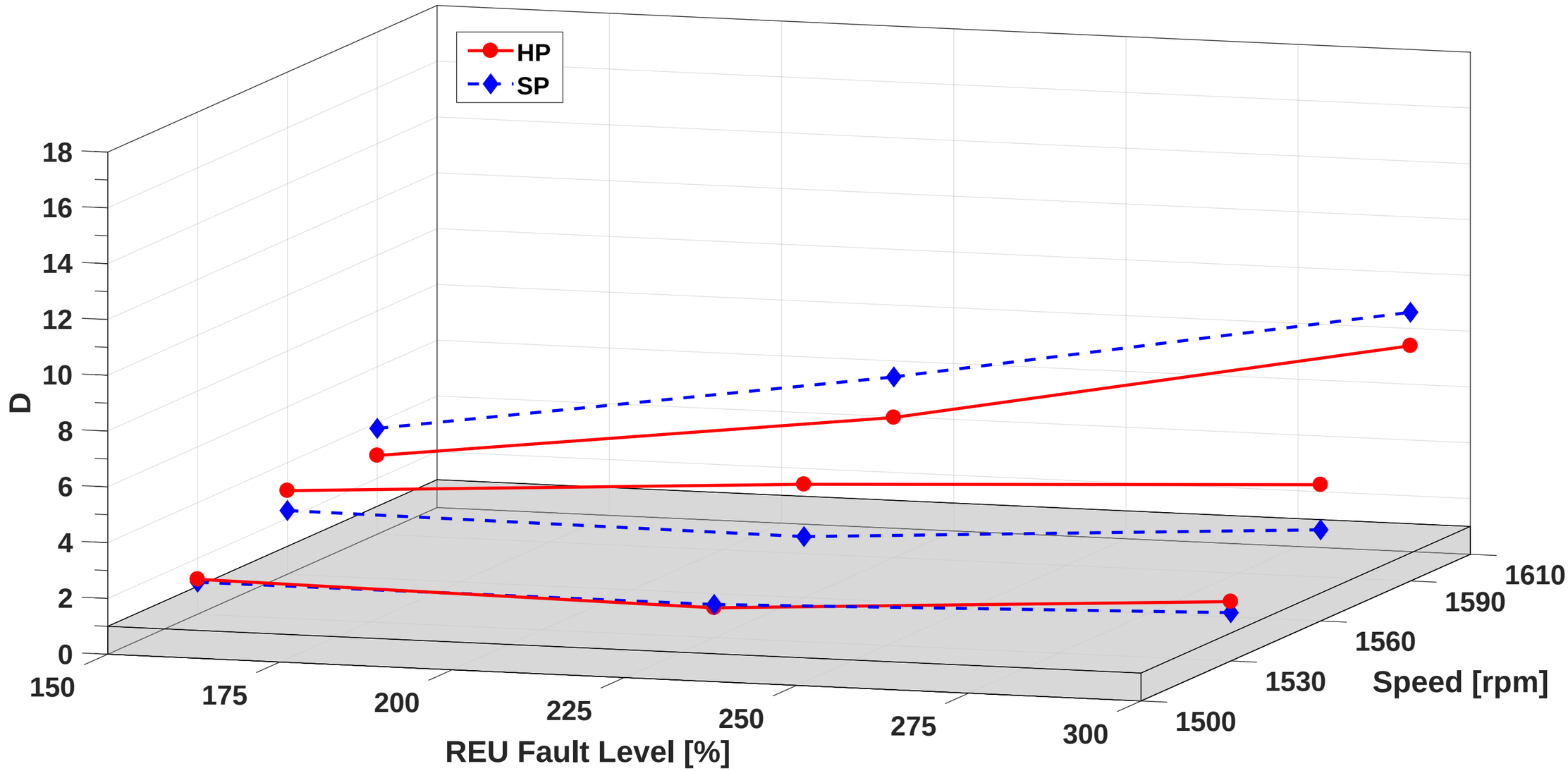
HP
SP
D
18
16
14
12
10
8
6
4
2
0
150
175
200
225
250
275
300
REU Fault Level [%]
1500
1530
1560
1590
1610
Speed [rpm]

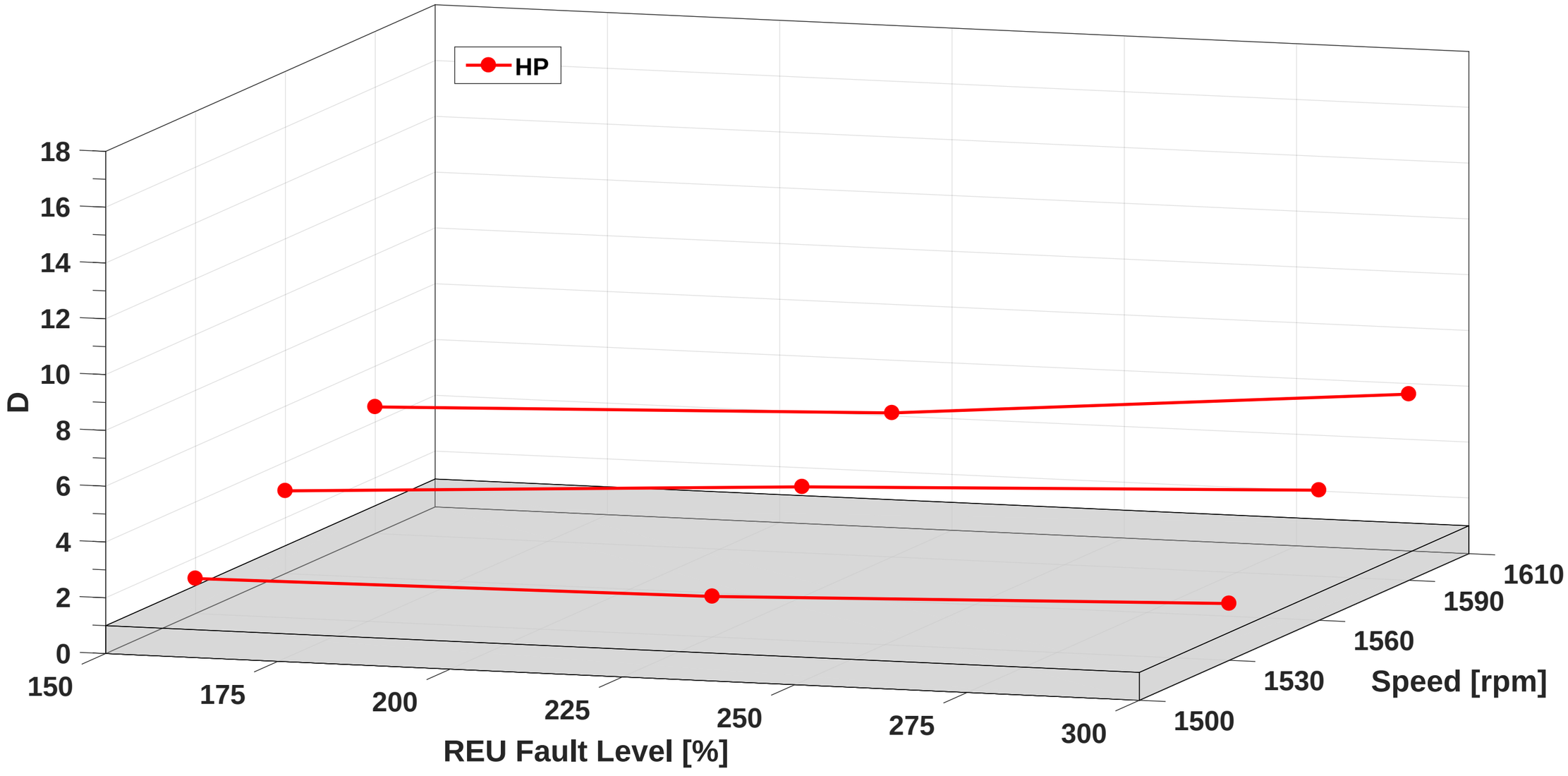
HP
18
16
14
12
10
8
6
4
2
0
D
150
175
200
225
250
275
300
REU Fault Level [%]
1500
1530
1560
1590
1610
Speed [rpm]

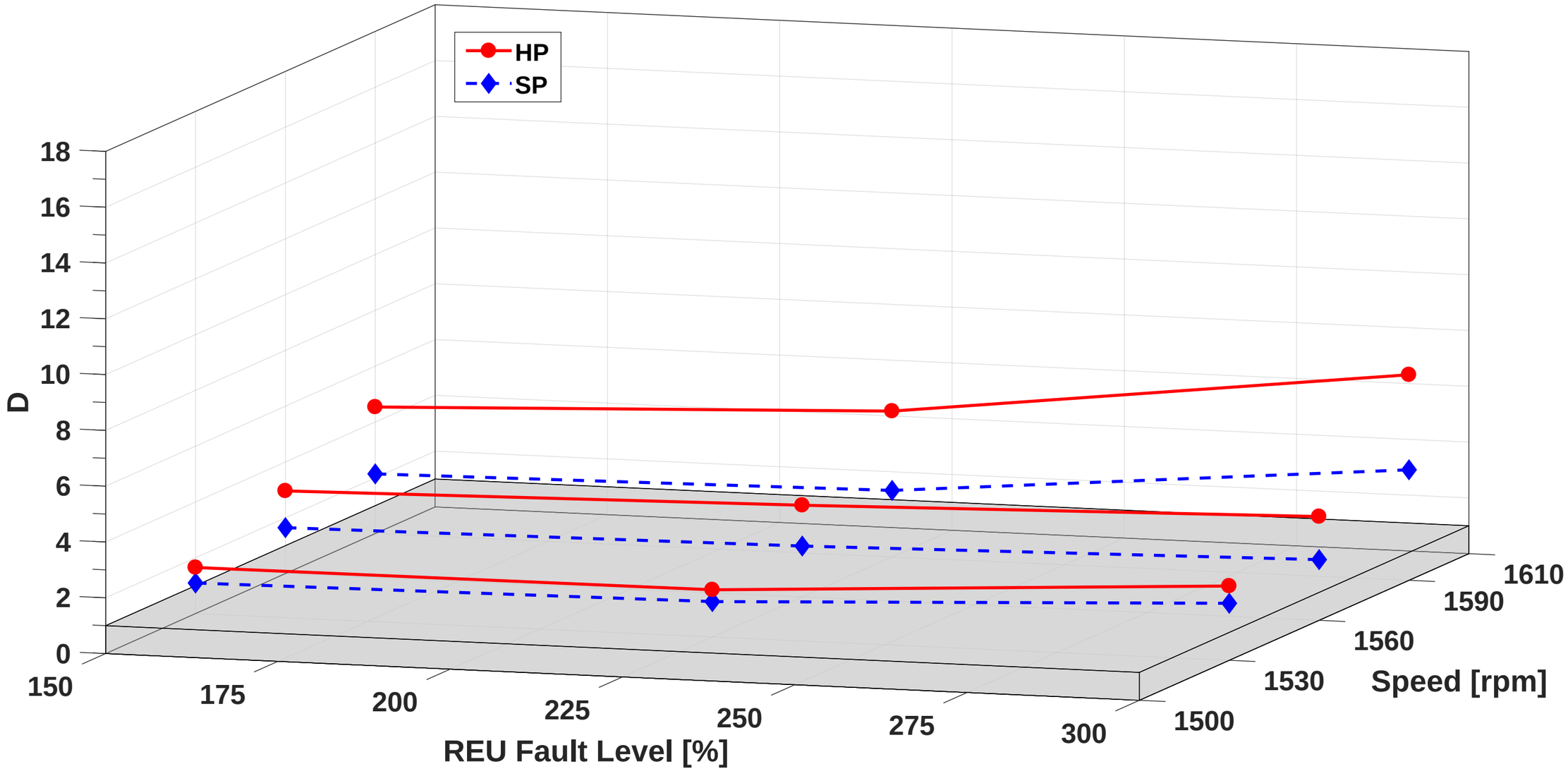
HP
SP
18
16
14
12
10
8
6
4
2
0
D
150
175
200
225
250
275
300
REU Fault Level [%]
1500
1530
1560
1590
1610
Speed [rpm]

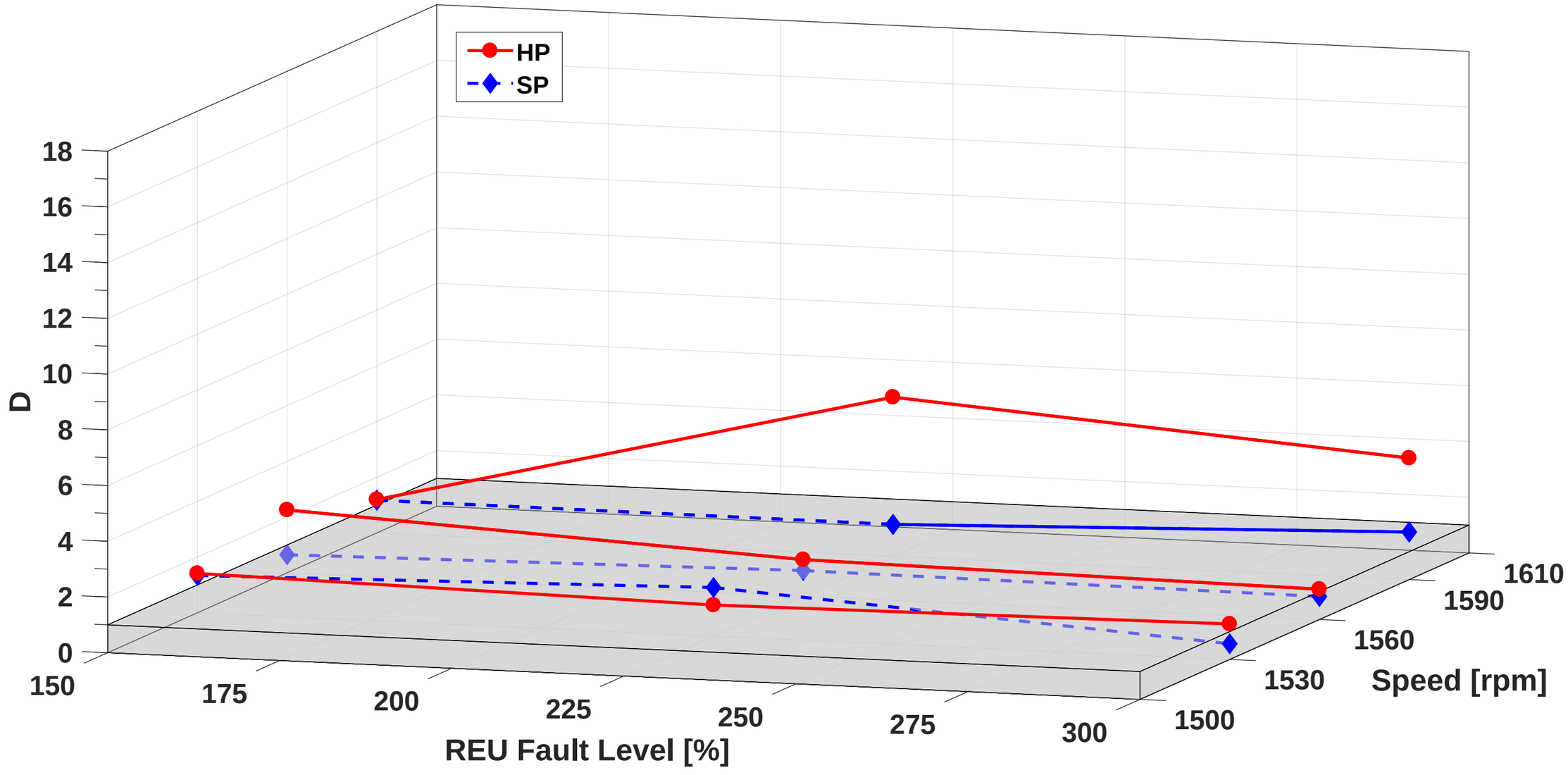
HP
SP
18
16
14
12
10
8
6
4
2
0
D
150
175
200
225
250
275
300
REU Fault Level [%]
1500
1530
1560
1590
1610
Speed [rpm]

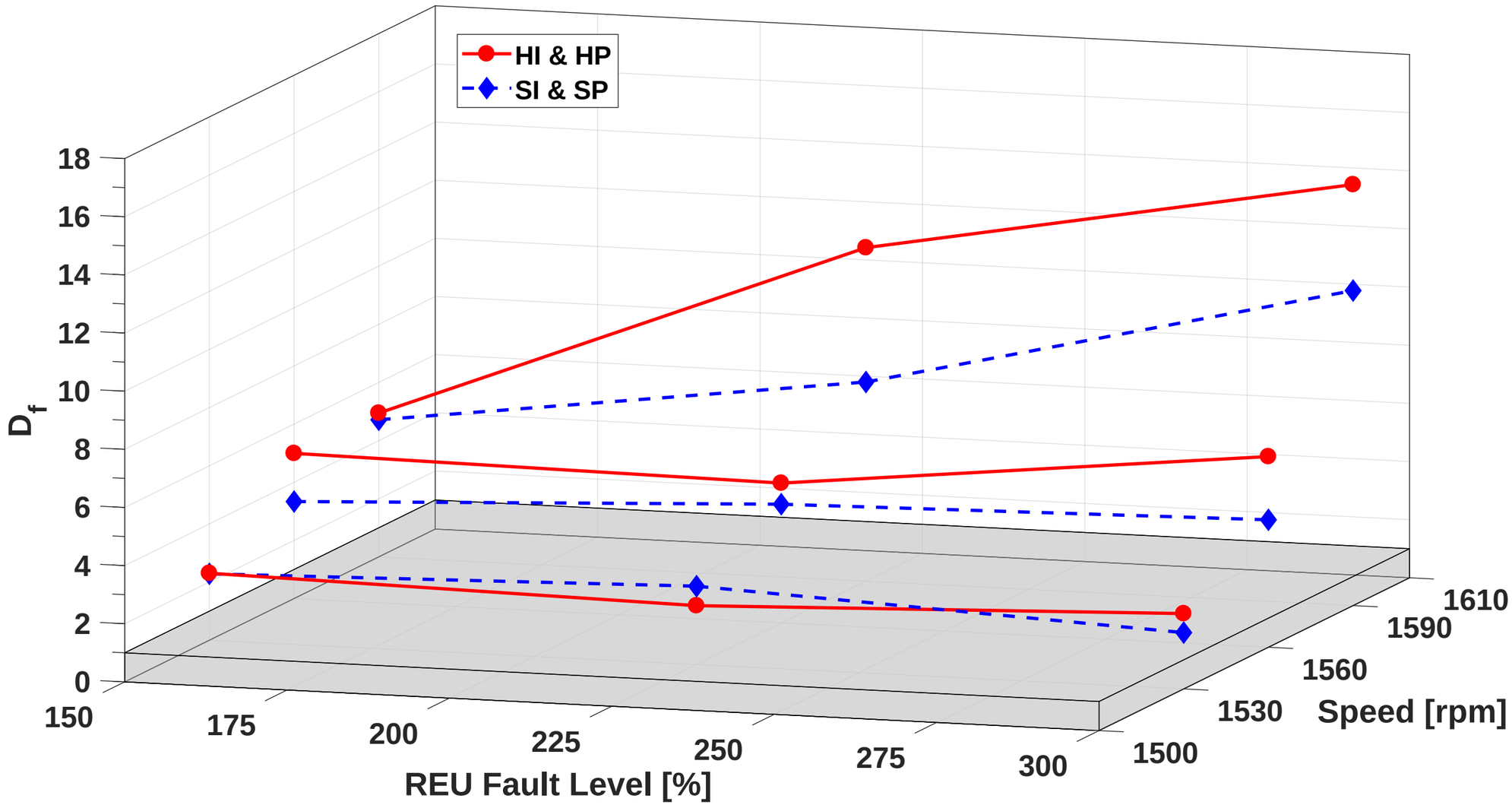
HI & HP
SI & SP
D_f
18
16
14
12
10
8
6
4
2
0
150
175
200
225
250
275
300
REU Fault Level [%]
1500
1530
1560
1590
1610
Speed [rpm]

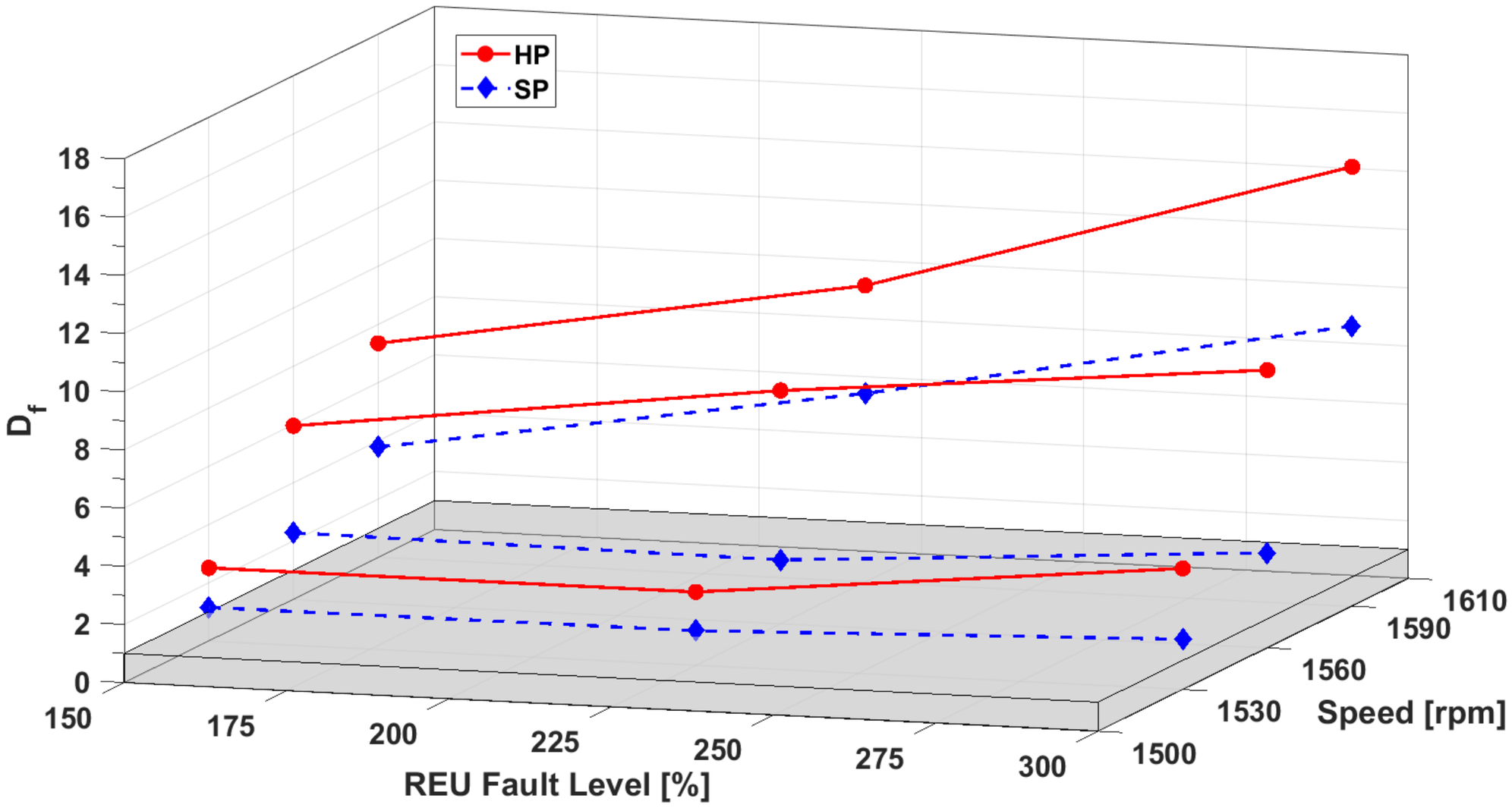
HP
SP
18
16
14
12
10
8
6
4
2
0
D_f
150
175
200
225
250
275
300
REU Fault Level [%]
1500
1530
1560
1590
1610
Speed [rpm]

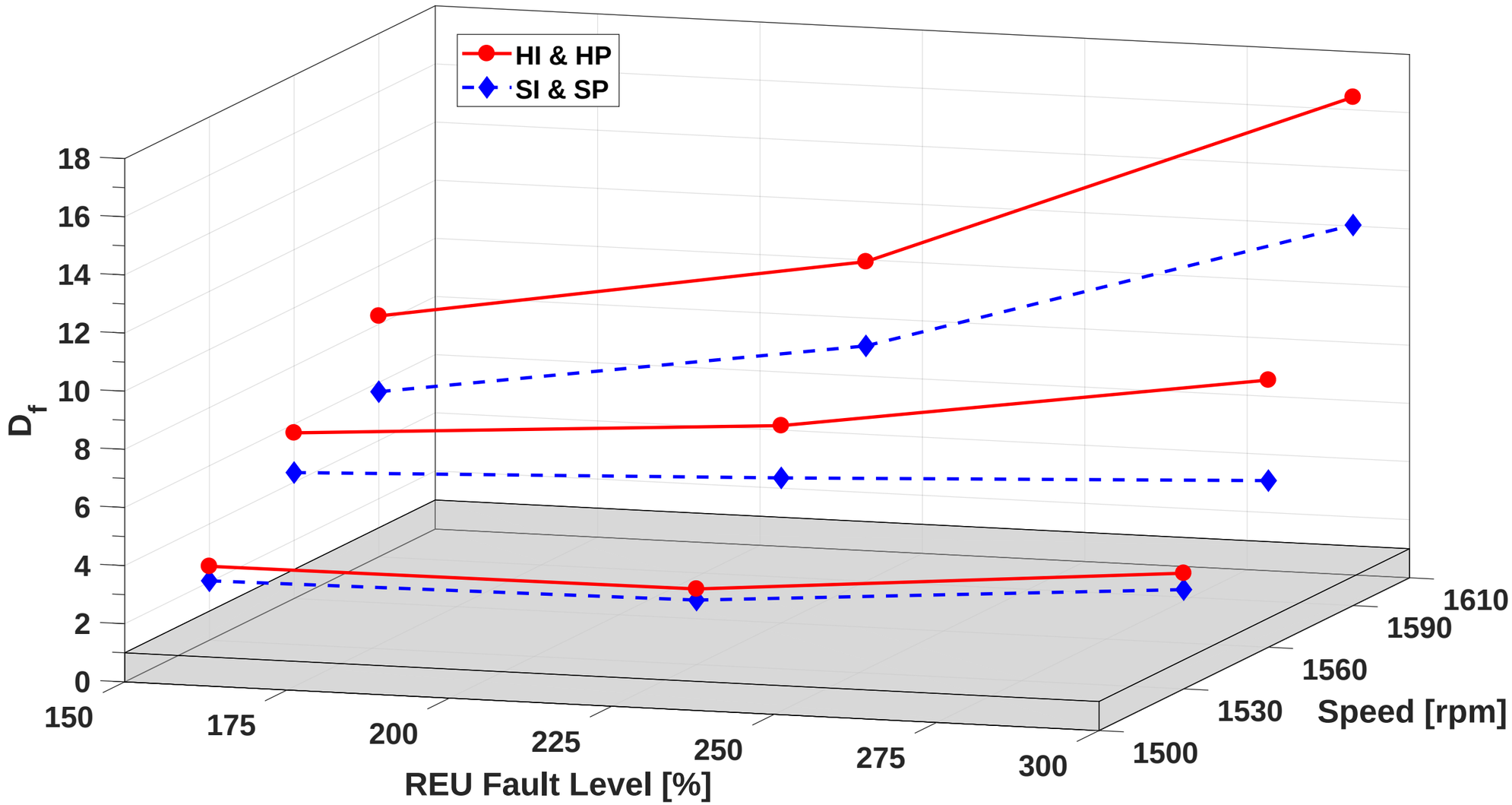
HI & HP
SI & SP
D_f
18
16
14
12
10
8
6
4
2
0
150
175
200
225
250
275
300
REU Fault Level [%]
1500
1530
1560
1590
1610
Speed [rpm]

ACCEPTED MANUSCRIPT

'Electrical & Mechanical Diagnostic Indicators of Wind Turbine Induction Generator Rotor Faults' by D. Zappalá, N. Sarma, S. Djurović, C. J. Crabtree, A. Mohammad & P. J. Tavner.

HIGHLIGHTS:

- Investigation of doubly-fed induction generators (DFIG) rotor electrical unbalance
- Comprehensive predictions and tests of electrical & mechanical signals
- Fault indicators for incorporation into wind turbine condition monitoring systems
- Additive data fusion preliminary analysis indicates improved fault detectability

ACCEPTED MANUSCRIPT